SCUBIDO: a Bayesian modelling approach to reconstruct palaeoclimate from multivariate lake sediment data

Laura Boyall[1], Andrew C. Parnell[2], Paul Lincoln[1], Antti Ojala[3,4], Armand Hernández[5], Celia Martin-Puertas[1].

[1.] Department of Geography, Royal Holloway University of London, Egham, TW20 0EX, UK.

[2.] School of Mathematics and Statistics, University College Dublin, Ireland.

[3.] Department of Geography and Geology, University of Turku, FI-20014, Finland

[4.] Geological Survey of Finland, Vuorimiehentie 5, FI-02151 Espoo, Finland

[5.] GRICA Group, Centro Interdisciplinar de Química e Bioloxía (CICA), Faculty of Sciences, Universidade de Coruña, Coruña, Spain.

Correspondence to: Laura Boyall (Laura.Boyall.2016@live.rhul.ac.uk)

Abstract

Quantification of proxy records obtained from geological archives is key for extending the observational record to estimate the rate, strength, and impact of past climate changes, but also to validate climate model simulations, improving future climate predictions. SCUBIDO (Simulating Climate Using Bayesian Inference with proxy Data Observations), is a new statistical model for reconstructing palaeoclimate variability and its uncertainty using Bayesian inference on multivariate non-biological proxy data. We have developed the model for annually laminated (varved) lake sediments as they provide a high-temporal resolution to reconstructions with precise chronologies. This model uses non-destructive X-Ray Fluorescence core scanning (XRF-CS) data (chemical elemental composition of the sediments) because it can provide multivariate proxy information at a near continuous, sub-mm resolution, and when applied to annually laminated (varved) lake sediments or sediments with high accumulation rates, the reconstructions can be of an annual resolution. whilst this model has been built for this proxy type, its flexibility means that the model could be applied to other multivariate proxy datasets.

SCUBIDO uses a calibration period of instrumental climate data and overlapping μXRF-CS data to learn about the direct relationship between each geochemical element (reflecting different depositional processes) and climate, but also the covariant response

33 between the elements and climate. The understanding of these relationships is then applied to
34 the rest of the record to transform the proxy values into a posterior distribution of palaeoclimate
35 with quantified uncertainties. In this paper, we describe the mathematical details of this
36 Bayesian approach and show detailed walk-through examples that reconstruct Holocene annual
37 mean temperature from two varved lake records from central England and southern Finland.
38 We choose to use varved sediments to demonstrate this approach as SCUBIDO does not
39 include a chronological module and thus the tight chronology associated with varved sediments
40 is important. The out-of-sample validation for both sites show a good agreement between the
41 reconstructed and instrumental temperatures emphasising the validity of this approach. The
42 mathematical details and code have been synthesised into the R package, SCUBIDO, to
43 simplify encourage others to use this modelling approach and produce their own
44 reconstructions. Whilst the model has been designed and tested on varved sediments, µXRF-
45 CS data from other types of sediment records which record a climate signal could also benefit
46 from this approach.

1.0 Introduction

48 Anthropogenic climate change over the most recent decades have heightened the need to look
49 beyond the instrumental period to find common patterns to both today's climate and future
50 climate projections (IPCC, 2023; Kaufman and McKay, 2022). This calls for chronologically
51 constrained, climate-sensitive proxy records to extend the understanding of climate variability
52 before the instrumental period. These reconstructions can be used to contextualise present
53 changes observed in the climate system, identify recurrent trends which are unable to be
54 observed in the short instrumental record (e.g. decadal-centennial variability), and be used as
55 potential analogues for future climate scenarios (Bova et al., 2021; Liu et al., 2020; Snyder,
56 2010). In addition, quantitative reconstructions provide the opportunity to perform climate
57 sensitivity experiments between proxy reconstructions and climate model simulations,
58 strengthening climate projections for the future (Kageyama et al., 2018; Burls and Sagoo, 2022;
59 Zhu et al., 2022).

60 The Holocene Epoch (11,700 years to present, where present is 1950 CE) has been the
61 focus of many proxy and modelling investigations (e.g. Liu et al., 2014; Bader et al., 2020;
62 Kaufman et al., 2020a; Bova et al., 2021; Erb et al., 2022). This time period experienced
63 temperatures which were similar to today, and the availability of proxy records makes the
64 Holocene a favourable interglacial to investigate climate variability across multi-millennial
65 timescales. Recently, there have been a number of new reconstructions of global temperature

which are based on large proxy dataset compilations (Kaufman et al., 2020a; Kaufman et al., 2020b; Osman et al., 2021; Erb et al., 2022). These synthesise different marine (Osman et al., 2021), or a combination of terrestrial and marine (Kaufman et al., 2020b) proxy records and either use statistical approaches (Kaufman et al., 2020a) or combine these with data assimilation (Osman et al., 2021; Erb et al., 2022) to reconstruct climate both spatially and temporally. These have provided great insight into climate variability across large spatial scales, of which are not possible when looking at individual site records. However, they all have a common limitation which is the temporal resolution of their reconstructions. Due to the nature of the proxies included in the large datasets (e.g. pollen, isotopes, foraminiera), the proxy signal is often non-continuous creating a median reconstuction resolution of ca. 100-200 years (Kaufman et al., 2020b). Whilst this temporal resolution is acceptable to look at spatially extensive and long-term climate variability across centennial to millennial timescales (Cartapanis et al., 2022), higher frequency variability such as the multi-decadal climate system is unable to be investigated, even though this is key to improve climate predictions within this century (Cassou et al., 2018). Erb et al. (2022) produced a global temperature reconstruction at a decadal resolution. However, they used the Temp12k dataset which only 11 out of the 1,276 records have a decadal, or higher temporal resolution, and some records having a resolution of up to 700 years (Kaufman et al., 2020b; Erb et al., 2022). This meant that in order for them to achieve a decadal reconstruction they have to leverage from transient climate simulations in a data assimilation approach to upscale their temporal resolution to decadal. Whilst a lot can be learnt from their reconstruction, using the transient simulations means that much of the decadal climate variability observed in this reconstruction would be forced by the model, rather than the proxy data itself.

Reconstructions of climate from a proxy record, whether this be a single-site, or a compilation of multiple sites, require a transformation from the qualitative climate information derived from proxy values to a quantified climate parameter with physical units of measurements (i.e. °C, mm of precipitation) (Chevalier et al., 2020). A number of statistical or mechanistic methods can be used, each with varying levels of complexity, uncertainties, and functionality (Tingley et al., 2012). Each method requires a calibration stage or training set relying on modern observations of the relationship between the proxy and climate which is then projected onto the proxy data (Juggins and Birks, 2012). Quantitative approaches have matured from rather simplistic methods including linear regression (e.g. Imbrie and Kipp, 1971), to methods of increased complexity such as weighted averaging regression (e.g. ter

99 Braak and Juggins, 1993; Liu et al., 2020), composite plus scaling (e.g. Jones et al., 2009;
100 Kaufman et al., 2020a), modern analogue techniques (e.g. Jiang et al., 2010), and artificial
101 neural networks (e.g. Wegmann and Juame-Santero, 2023) which are summarised well in
102 Chevalier et al. (2020). Interpreting the palaeoclimate record and reconstructing climate can be
103 complex and often faced with several challenges including uncertain chronologies,
104 assumptions in proxy formation and preservation, and non-stationary relationships between the
105 climate system and proxy response through time (Sweeney et al., 2018; Cahill et al., 2023).
106 This is especially true when the archives used to reconstruct climate have faced significant
107 alterations due to rising anthropogenic activity over the last several thousands of years,
108 questioning the stationarity of proxy-climate relationships. Each of these complexities have led
109 to a greater reliance on hierarchical statistical approaches, such as Bayesian statistics to
110 reconstruct climate through time (Tingley et al., 2012).

111   Bayesian statistics is an approach based on Bayes' Theorem and can be summarised as
112 applying prior knowledge to update the probability of a hypothesis when new data becomes
113 available (van de Schoot et al., 2021). It has been used to answer many statistical problems
114 which has included reconstructing palaeoclimate (e.g. Haslett et al., 2006; Parnell et al., 2015;
115 Tierney et al., 2019; Cahill et al., 2023). Many frequentist (non-Bayesian) approaches to
116 reconstruct climate mentioned previously often struggle to capture the complex relationships
117 inherent between climate and proxy data. This occurs when the learnt relationship in the
118 calibration interval or training data is fixed, and then applied directly onto the palaeo data which
119 results in the assumption of a stationary relationship through time, and fixed uncertainty
120 estimates (Birks et al., 2012; Sweeney et al., 2018; Zander et al., 2024). However, we argue
121 that climate often exhibits non-stationary behaviour and this needs to be captured in the chosen
122 model. By contrast, a Bayesian approach allows a continued update about the belief of the
123 relationship between the proxy, the climate, and associated parameters (Chu and Zhao, 2011).
124 In addition, Bayesian analysis can holistically account for different sources of uncertainty
125 influencing a reconstruction (Birks et al., 2012; Sweeney et al., 2018). Bayesian methods can
126 consider the uncertainties at all stages of the modelling process and model these as joint
127 probability distributions producing properly quantified uncertainties with credible intervals
128 (Tingley and Huybers, 2010; Sweeney et al., 2018; Cahill et al., 2023).

129   A rising number of studies have used a Bayesian framework in their climate
130 reconstructions (e.g. Haslett et al., 2006; Holmström et al., 2015; Parnell et al., 2015; Tierney
131 et al., 2019; Hernández et al., 2020; Cahill et al., 2023). However, they provide low temporal
132 resolutions as they are based on non-continuously sampled proxies, resulting in reconstructions

of climate across multi-decadal to centennial timescales. This calls for a greater number of quantified climate reconstructions using hierarchical modelling from records with refined chronologies and proxies sampled at a high resolution.

Micro X-ray Fluorescence core scanning (μXRF-CS hereafter) is a non-destructive approach which provides multivariate information about the geochemical composition of marine and lacustrine sediment cores (Davies et al., 2015). The geochemical information produced by μXRF-CS provides relative changes in the element abundance (Bertrand et al., 2024). Unlike alternative geochemical proxies (e.g. stable isotopes) or biological proxies (e.g. pollen, foraminifera) which require discrete sampling, the μXRF-CS approach scans sediment sequences continuously enabling the proxy data to be produced at very high sampling resolutions (up to 0.2 mm). When this approach is applied on sediment sequences with either sufficient sedimentation rates (>0.5 mm per year) or annual laminations (varves) (Zolitschka et al., 2015), it can provide proxy information at a seasonal to decadal timescale. μXRF-CS has mostly been used to qualitatively reconstruct palaeoenvironments, as the relative changes in geochemical composition of sediments are a direct response to the changing climatic and environmental conditions in the lake-catchment system (Peti and Augustinus, 2022).

Our main goal here is to combine the advantages of using Bayesian inference in climate reconstructions with the palaeoclimate value of varved records. In this methods-based paper we aim to i) present a Bayesian approach to transform multivariate μXRF-CS data into a quantitative palaeoclimate dataset, ii) demonstrate the applicability of this approach on two varved lake records from Europe, iii) compare the output of the Bayesian model to previously published reconstructions to test the climatic reliability, and iv) promote its use through the user-friendly R package, SCUBIDO.

2.0 Methods

2.1 Proxy data

The modelling approach has been built for the use of μXRF-CS data as the chosen proxy. Raw μXRF-CS data originates in the form of element intensities which is often non-linear to the concentration of elements in the sediment and can also be affected by the sediment's physical properties, measurement time and sample geometry, therefore we use centred-log ratios (clr hereafter) to mitigate against these problems (Aitchison, 1986; Tjallingii et al., 2007; Weltje and Tjallingii, 2008; Weltje et al., 2015; Dunlea et al., 2020). Transforming raw elements to

clr-elements requires a dataset with minimal low or null counts (Bertrand et al., 2024). Therefore, elements with excessive null values should be removed before performing the transformation. Following this, this approach does not assume that any element has a stronger relationship with climate thus, we pass all elements which were able to be clr-transformed to the model.

2.3 Bayesian framework

For our quantitative reconstruction of climate given the µXRF-CS proxy data, we use Bayesian inference and base our framework on the modelling approach described in Parnell et al. (2015) and Hernández et al. (2020). Below we outline the notation used throughout:

- C is used to represent the value of the climate variable at each time point.
- We use XRF_{ij} to indicate the centred-logged transformed µXRF-CS data at each depth of the sediment core (i) where $i = 1, ..., n$ depths. As the µXRF-CS data is multivariate, j reflects the number of different centred log ratio transformed elements ($j = 1, ..., n$ elements).
- t_i denotes the calibrated age (t) of each depth (i) in cal years BP (before present where present refers to 1950). It is important to note that SCUBIDO does not contain a geochronological module and thus age uncertainty is not considered in this modelling approach.
- θ is used to represent the parameters ($\mu, \beta_0, \beta_1, \beta_2$) which govern the relationship between each of the µXRF-CS elements at each time point and the climate variable. These are subscripted with j to denote the element to which they refer to.
- σ_c is used to represent the standard deviation of climate per unit of time for our random walk model detailed in this paper.
- A superscripted m and f are applied to each of the variables when referring to the modern and fossil data sets respectively. For example, C^m equates to the modern climate, and XRF^f refers to the fossil µXRF-CS data.

More definitions of variables and model parameters used in the model framework are presented in Table S1.

The Bayesian posterior distribution we aim to estimate is outlined below:

(1)

196 $$p\left(C^f, \theta, \sigma_c | XRF^f, C^m, XRF^m\right) \propto p(XRF^m | C^m, \theta) \cdot p\left(XRF^f | C^f, \theta\right) \cdot p(C^f, C^m | \sigma_c)\, p(\sigma_c)\, p(\theta).$$

The posterior distribution on the left side of the equation $p\left(C^f, \theta, \sigma_c | XRF^f, C^m, XRF^m\right)$, represents the probability distribution of the fossil climate given fossil and modern μXRF-CS data, and modern climate. We use the likelihood expression $p(XRF^m | C^m, \theta)$, to represent the calibration period where we learn about the relationship between the μXRF-CS data and climate variable, discussed in more detail in Sect. 2.3.2. $p(XRF^f | C^f, \theta)$, then represents the likelihood of the fossil data given the climate, and finally $(C^f, C^m | \sigma_c)$, represents the prior distribution associated with the fossil climate and its dynamics over time.

2.3.1 Model fitting

To fit the above model, we follow the computational shortcut of Parnell et al. (2015) which assumes that all the information about the calibration parameters (θ), comes from the modern data. This means that the model is fit in two parts, with the first being the estimation of θ within a calibration period, and then the second part which estimates the fossil climate (C^f) and σ_c. Thus, the resulting model becomes:

(2)

213 $$p\left(C^f, \theta, \sigma_c | XRF^f, C^m, XRF^m\right) \propto p(\theta, \sigma_c | XRF^m, c^m) \cdot p\left(XRF^f | C^f, \theta, \sigma_c\right) \cdot p(C^f, C^m | \sigma_c)\, p(\sigma_c).$$

The first term on the right-hand side is estimated separately and represents the posterior distribution of the modern calibration relationship parameters which is then not further learnt from the fossil data in the second part of the model fit. Given the different parts of the modelling approach, we split the following section into two, firstly fitting the modern calibration period (Section 2.3.2), and then secondly using what is learnt from this stage to reconstruct fossil climate (Section 2.3.3).

2.3.2 Calibration model fitting

Like all quantitative transformations of palaeoclimate, the first step is to understand the relationship between the proxy and the climate variable. In our modelling approach this relationship is learnt from the first term on the right-hand side of Equation 2 ($p(\theta, \sigma_c | XRF^m, c^m)$) and includes not only the causal relationship between the individual μXRF-CS elements and climate, but also the covariance between the elements. The data used

228   for this section of the model is the most recent period and must be aligned with an overlapping

229   period of instrumental climate (C^m) and we call this our calibration dataset.

230   This step assumes that some of the variability observed in the proxy data is controlled

231   by the climate variable, this is sometimes referred to a 'forward' model. Here we want to

232   estimate the posterior distribution of the θ parameters ($\beta_0, \beta_1, \beta_2, \mu_0$), and the climate

233   variability parameter σ_c, from a joint probability distribution using the following:

234   (3)

235
$$p(\theta, \sigma_c | XRF^m, C^m) \propto p(XRF^m | C^m, \theta) \cdot p(C^m | \sigma_c) \cdot p(\theta)\, p(\sigma_c).$$

236

237   We use $p(\theta)$ to represent the prior distribution of the parameters $\beta_0, \beta_1, \beta_2, \mu_0,$ with σ_c

238   and $p(C^m | \sigma_c)$, representing the prior distribution on modern climate (we use a random walk

239   with standard deviation σ_c at each time point). $p(XRF^m | C^m, \theta)$ is our likelihood distribution,

240   and finally the parameter's posterior distribution is represented by $p(\theta, \sigma_c | XRF^m, C^m)$.

241   To approximate the relationship between the clr-transformed μXRF-CS data and the

242   climate, we use a multivariate normal polynomial regression model for each of the μXRF

243   elements:

244   (4)

245
$$XRF_i^m \sim MVN(M_i, \Sigma)$$

246
$$M_i = [\mu_{i1}, \mu_{i2}, \ldots, \mu_{i11}]$$

247
$$\mu_{ij} = \beta_{0j} + \beta_{1j} \cdot C(t_i) + \beta_{2j}\, C(t_i)^2.$$

248

249   The mean term μ_{ij} captures the relationship between climate and assumes a quadratic

250   relationship with a single mode when $\beta_{2j} < 0$. We use Σ to represent the covariance matrix of

251   the relationship between each of the different elements which are not explained by μ_{ij}. We

252   acknowledge that other more complex models could be used to fit the relationship between the

253   climate and the μXRF-CS elements rather than a polynomial model explained here. However,

254   when experimenting this with a more complicated P-spline model we experienced overfitting

255   and a significant reduction in the computational speed, whereas the polynomial regression

256   model is sufficient to capture the relationships between the elements and climate without

257   having a large computational burden.

258   Vague normal distributions are used for the priors on $\beta_0, \beta_1,$ and β_2, an inverse Wishart

259   prior on Σ, and finally a vague uniform prior distribution for σ_c:

260   (5)

$$B_{oj} \sim N(0,100), B_{1j} \sim N(0,100), B_{2j} \sim N(0,100)$$

$$\Sigma^{-1} \sim Wishart(R, k+1).$$

For the prior distribution on climate, we use a continuous time random walk:

$$\text{(6)}$$

$$P(C_i^m) \sim N(C_{i-1}^m, \omega_i)$$

$$\omega_i = (t_i^m - t_{i-1}^m) \cdot \sigma_c^2.$$

We give σ_c a vague uniform distribution: $\sigma_c \sim U(0,100)$. The choice behind using vague priors in this part of the model is what we do not want to make any assumption about the relationship between the µXRF-CS elements and climate and instead allow the model to learn about the data itself.

2.3.3 Fossil model fitting

Once the model has learnt about the relationship between the µXRF-CS data and climate, the second part of the computational shortcut can commence (Parnell et al., 2015). This first involves using the learnt relationship from the calibration period to create marginal data posteriors (MDPs) which represent all the information about fossil climate contained in one layer of µXRF data. Thus, we initially estimate the C^f using only the information within a particular time slice (XRF^f). Using only the information from one time slice at a time allows the model to marginalise over the parameters (θ) and reduce the dimensionality of the data. This step decreases the computational burden of estimating both the climate-proxy relationship and the fossil climate values in the same step. Information on the MDP fitting can be found in S2 and in more detail in Parnell et al. (2015; 2016).

To accurately capture the climate dynamics of the fossil period, we include a more informed prior for the random walk of fossil climate by re-using the continuous time random walk from the modern calibration module and combine each of the individual MDP layers once they are corrected. This enables us to create a complete joint posterior distribution of the combined C^f and C^m and fit the model detailed in Equation 2. As above, the varying time steps are captured via a dynamic precision term:

$$\text{(7)}$$

$$P\left(C_i^f\right) \sim N(C_{i-1}^f, \omega_i)$$

$$\omega_i = \left(t_i^f - t_{i-1}^f\right) \cdot \sigma_c^2.$$

To fully learn the climate dynamics standard deviation parameter from both the fossil and the modern data we set a log-normal prior distribution for σ_c:

$$\sigma_c \sim \text{LN}(a, b). \tag{8}$$

The values a and b are chosen to match the posterior distribution from the modern calibration model fit.

The model produces an ensemble of posterior climate paths that cover the fossil and modern periods. This considers the uncertainties in the µXRF-CS proxy climate relationship with a mild smoothing constraint arising from the random walk prior. The ensemble can then be summarised by taking the median value of the posterior distribution C^f and calculating the 50% and 95% credible interval of the reconstruction using the 2.5%, 25%, 75%, and 97.5% percentiles for plotting.

Section 3.0 Walk through example

This next section of the paper provides a walk-through example of each stage of the Bayesian model fitting on real life µXRF-CS data. In an attempt to make this modelling approach as user-friendly as possible, we have produced the R package SCUBIDO (Simulating Climate Using Bayesian Inference with proxy Data Observations) which synthesise the modelling process into several distinct steps. The package can be downloaded from the GitHub repository: https://github.com/LauraBoyall/SCUBIDO alongside a walk-through example and a link to a video tutorial on how to use the R package.

We first demonstrate this example on the lake sediments of Diss Mere, a small lake in the UK containing Holocene varved sediments. This site has been chosen due to the sediments being annually laminated for much of the Holocene (from 10 to 2 thousand years before 1950 CE, cal. BP hereafter); it therefore has a refined chronology based on annual layer counts with age uncertainties of less than a few decades (Martin-Puertas et al., 2021), which is important for this modelling approach as we do not model or consider chronological uncertainty. The averaged sedimentation rate for the varved sequence is 0.4 mm/year with variability between 0.1 and 1.8 mm/year (Martin-Puertas et al., 2021). The most recent two millennia are recorded

327 in the top 9 m of the sediment sequence, where the annual laminations are poorly preserved,
328 and counting was not possible. However, the chronology has been constrained through a series
329 of radiometric dating techniques (^{14}C, ^{137}Cs) and tephrochronology, providing a high average
330 sedimentation rate of ca. 0.5 cm/year and described in detail in Boyall et al. (2024) and
331 summarised in S3. Both the modern sediment depositional processes, and palaeo sediments
332 have been studied in detail through modern lake monitoring, microfacies analysis and analysis
333 of the μXRF-CS record, which all highlighted that the main environmental processes
334 explaining the sediment deposition in the lake has not changed through time and respond to
335 climate variations on seasonal to multi-centennial timescales (Boyall et al., 2023; Martin-
336 Puertas et al., 2023; Boyall et al., 2024). Whilst human activity had an impact on the lake
337 sedimentation in the last 2,000 years, i.e. increased detrital input into the lake (Boyall et al.,
338 2024), the lake sedimentation and sediment composition keeps responding to the annual lake
339 cycle (monomictic), which is driven by climate parameters such as temperature and wind speed
340 (Boyall et al., 2023). The sensitivity of these sediments to weather and climate variability thus
341 provides scope for testing this modelling approach.

342 The Diss Mere sediments were scanned using an ITRAX μXRF-Core scanner (Cox
343 Analytical Systems) at the GFZ-Potsdam and geochemical elements include Si, S, K, Ca, Ti,
344 V, Mn, Fe, Rb, Sr and Zr at 200 μm resolution with a dwell time of 6 s and was later resampled
345 to 400 μm for processing (Boyall et al., 2024). These elements were chosen based on having a
346 standard error <15% (Boyall et al., 2024), and not too many null values to perform the clr
347 transformation (Bertrand et al., 2024).

348 Boyall et al. (2024) found a good visual relationship between the μXRF-CS data,
349 specifically the element calcium (Ca) (linked to temperature-induced authigenic calcite
350 precipitation deposited during spring to early Autumn), and annual mean temperature evolution
351 through the Holocene (Davis et al., 2003; Kaufman et al., 2020a; Rasmussen et al., 2007).
352 Whilst this study found the strongest relationship to climate with Ca, all the elements are used
353 in this modelling approach given that SCUBIDO models the covariance between the elements
354 and learns from these relationships. For the first two thousand years of the geochemical record
355 between ca. 10,300 cal a BP and 8,100 cal a BP, the environmental interpretation of the element
356 data reflected a non-climate, local signal associated with the stabilisation of the lake
357 depositional environment during the early Holocene (Boyall et al., 2024). Therefore, we
358 attempt this modelling approach on only the geochemical data from 8,100 cal a BP to present.
359 We emphasise to future users of SCUBIDO that they should also conduct a qualitative analysis

of the μXRF-CS data and environmental interpretation prior to using SCUBIDO to ensure that their record is climate sensitive and has not been subjected to significant alterations from human activity.

3.1 Data set up

One of the most fundamental considerations for any type of palaeoclimate reconstruction is the choice of climate variable to reconstruct (e.g. annual mean temperatures, precipitation, growing season) given that different proxies are sensitive to a number of climate drivers (Sweeney et al., 2018). The SCUBIDO modelling approach can be easily adapted to reconstruct different climate parameters with overlapping instrumental data. However, it is important to note that not all lakes are responsive to every climate parameter of interest and thus the outputs may not be useful. For example, we attempted to run SCUBIDO on the Diss Mere μXRF-CS data to reconstruct both annual mean temperature and precipitation. However, the SCUBIDO output for precipitation from Diss Mere was not successful as the reconstruction was completely flat, not resembling precipitation variability and there was no predictive power between the elements and instrumental precipitation. Annual mean temperature on the other hand worked well, which support the temperature signal recorded in the μXRF-CS data during the Holocene (Boyall et al., 2024). Another point to highlight at this stage is that we run the Bayesian model using a multivariate dataset made of the elements measured by the μXRF scanner. We do so to avoid any bias through time as the climate-proxy relationship might not be stable over time. SCUBIDO also includes the relationship between elements (covariance) to deal with this issue. As the top of the μXRF-CS data (most recent period of sediment accumulation) begins at 1932 CE, a long-term instrumental temperature data set was required to get a sufficient length for the model to learn about the climate - proxy relationship. We therefore rely on the Hadley Central England Temperature (HadCET, Met Office) data which is the longest monthly temperature dataset available. However, it is worth noting that whilst this is the best instrumental record that we could use for Diss Mere given the long record, the meteorological stations used in this period of the record are not proximal to the site, and therefore some of the local temperature changes which are recorded in the proxy record, may not have been recorded by the meteorological station or vice versa.

The first step was to divide the data into two: the modern calibration dataset (containing an age index (t), modern μXRF-CS data (XRF^m) and the overlapping instrumental climate data (C^m)), and then the fossil data (containing the age (t) and μXRF-CS data for the remaining

data (XRF^f)). As there are many μXRF-CS data points per year we linearly interpolated the data to resample to annual means and align the XRF^m dataset with the corresponding year in the HadCET dataset. We begin the calibration dataset at 1700 CE, and the top of the μXRF-CS data finishes at 1932 CE, and because of a short gap where there was no μXRF-CS data present, it meant that the calibration dataset was 193 years long. Temperatures were converted into anomalies from the mean of the calibration period as this not only removes the arbitrary mean of the temperature reconstruction making the data more comparable, but it can also better constrain the climate values that the model can predict (see S2). The fossil data was provided in its original temporal resolution ranging between 5 data points per year to >25 data points per year depending on the sediment accumulation rate. This resulted in 59,461 time slices covering the period between 8,100 cal a BP and 1699 CE.

We check the model convergence using $\hat{R}$ values (Gelman and Rubin., 1992; Brooks and Gelman., 1998) and evaluate the performance of the model using both in sample and out-of-sample posterior predictive calibration checks (Gelman et al., 2008). We detail this analysis in more detail below.

3.2 Model fitting

The full model was run within the SCUBIDO R package. This package depends on JAGS (Just Another Gibbs Sampler, Plummer, 2003) through the R package 'R2jags' (Su and Yajima, 2021) to fit the modern calibration model and part of the fossil modelling stage. We ran the calibration model for 100,000 iterations and ignored the first 40,000 runs to allow the model to settle. We repeated this process four times using different starting values to run the MCMC in parallel. The $\hat{R}$ values were consistently <1.05 indicating that the algorithm had successfully converged during the Markov Chain Monte Carlo (MCMC) process (Gelman and Rubin., 1992; Brooks and Gelman., 1998. Vehtari et al., 2021; Su and Yajima, 2021). Fig. 1 shows the quadratic relationships between the individual μXRF-CS elements and temperature in the calibration period.
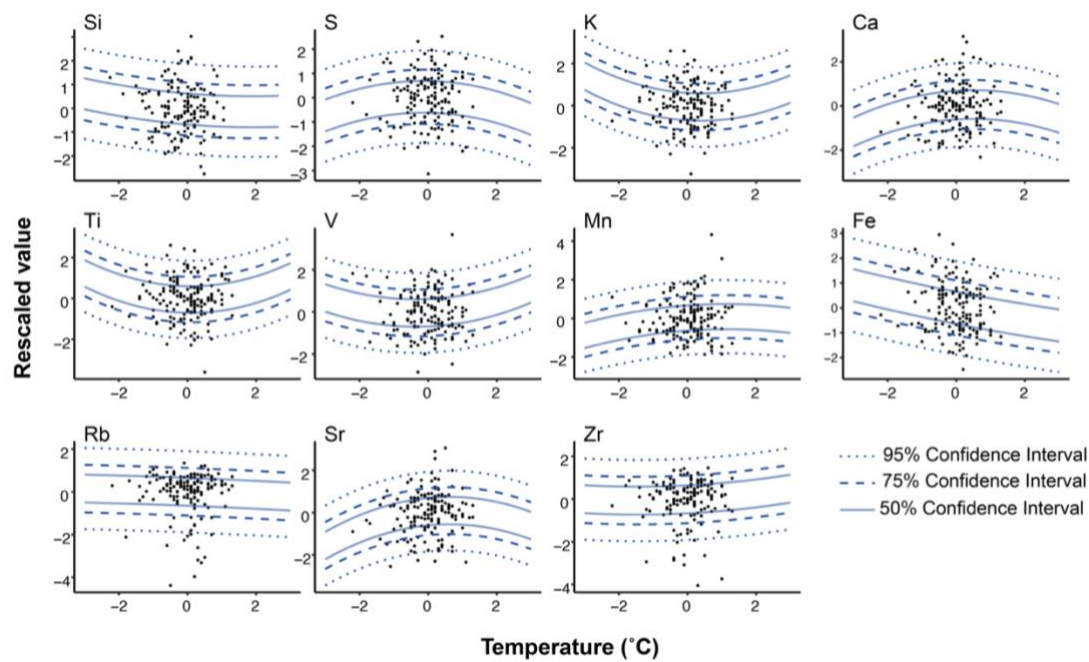
426

Figure 1: Relationship between the μXRF-CS elements and instrumental annual mean temperature from the calibration period. Individual μXRF-CS elements plotted against the instrumental climate anomaly data for each year. The quadratic relationships are represented by the lines with the solid lines representing the uncertainty ranges of 50%, 95% (dotted), 75% (dashed). Note that this modelling approach uses multivariate response regression however these plots display the individual response between each element and climate, hence the weak relationships plotted.

427

428   In more conventional approaches where μXRF-CS data is used to qualitatively
429   reconstruct climate, only one element, or pair of elements (in the form of a ratio) is used at a
430   time to reconstruct climate (for example Zander et al., 2024). This would be equivalent to our
431   approach if had we used a diagonal structure for $\sum$ (Equation 4). Such a diagonal structure
432   treats every element as independent and therefore may falsely reduce the uncertainty in the
433   resulting reconstructions. However, the novel contribution of our model is that it includes a
434   multivariate response regression approach that also models the covariances between the
435   elements, and so we argue produces more realistic, but also more uncertain reconstructions.
436   This explains why Fig. 1 shows only weak relationships between the individual 11 elements
437   and temperature. When each of these relationships are combined in the multivariate response
438   regression it provides a more precise posterior estimate of climate.
439   The fossil reconstruction stage for Diss Mere used 2,000 iterations and ignored the first
440   200 runs and repeated this process four times. Fewer iterations are required for this stage for
441   convergence as the model complexity is substantially reduced compared to the modern
442   calibration stage as MDPs are used. $\hat{R}$ values were <1.05 indicating satisfactory convergence

443 of the algorithm. The full reconstruction using all the SCUBIDO functions took approximately
444 16 hours on a standard computer using a single core.
445

3.3 Model validation

447 As a more rigorous test of the model performance, and to maximise the use of the palaeoclimate
448 reconstructions for climate services and model calibration, we further test its uncertainty
449 calibration properties using an out-of-sample five-fold cross validation routine (Mauri et al.,
450 2015; Chevalier et al., 2020). We removed 20% of the modern data and re-fit the full model to
451 obtain posterior estimates of the climate variable for years which the model has not seen during
452 the training phase. We repeated this step five times such that each observation year is removed
453 once. We can then compare these out-of-sample predicted climate values with the true values
454 in the modern data and see how often their uncertainty ranges cross with the true values. For
455 example, in an ideal model 95% of these values would lie within the 95% interval and 50% in
456 the 50% interval etc. Though in real-world data, the estimated proportion inside the credible
457 intervals may be slightly higher or lower, out-of-sample evaluation of climate reconstructions
458 seems not to be a common feature in the literature, but we would strongly advocate this in the
459 future, especially if a goal is for the reconstructions to be used beyond the palaeoclimate
460 community to, for example, help constrain climate model simulations.

461   The results of the five-fold cross validation showed that in 97.4% of the 193 calibration
462 temperatures, the reconstructions fell within the 95% credible interval (Fig. 2). The coverage
463 percentage for each individual fold ranged by 5.4%, from 94.6% to 100%. This demonstrates
464 the validity of the modelling approach and shows that most of the temperature variability
465 observed in the instrumental record is captured within the confidence intervals of the
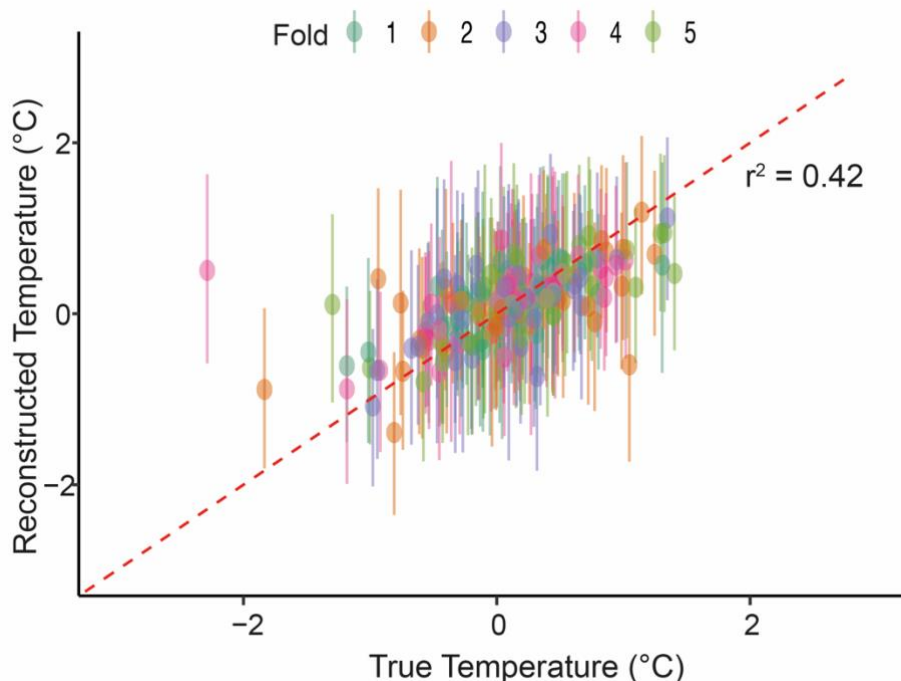466 reconstructed climate.

467

Figure 2: Results from the out-of-sample validation with true instrumental temperatures and reconstructed temperatures. Coloured dots represent the temperature values and error bars represent the predicted temperature's 95% uncertainty interval for each of the five folds. Note that the red dashed line is not the regression line and instead reflects the 1:1 relationship between true and reconstructed temperatures.

468

469   The coefficient of determination (r^2) for the true and reconstructed temperature is 0.42
470   (P = < 0.001), which suggests that there is some skill in the model prediction of the median
471   values, however it does suggest that not all the median values perfectly align with the true
472   instrumental temperature. This is not uncommon for palaeoclimate reconstructions, especially
473   as we are comparing proxy data that can also be affected by non-climate factors, such as human
474   activity and internal lake processes. In addition, we are using instrumental temperature data
475   which is not located proximal to the lake and contains large uncertainties, especially in the
476   earliest years of the HadCET dataset (Parker et al., 2010). Nevertheless, the coverage
477   percentage and overall good fit of the model can provide a reasonable assumption of the
478   validity of this approach.

479   **Section 4.0 Annually resolved annual mean temperature reconstructions in**
480   **Europe**

481   **4.1 Case site 1: Diss Mere, Central England**

482

The reconstruction of annually resolved temperatures for the past 8,100 cal a BP given the µXRF-CS from Diss Mere using Bayesian inference is presented in Fig. 3. The median Holocene temperature reconstructed from Diss Mere is 9.65 °C and has a maximum range of 1.68 °C with temperature anomalies between -1.26 °C and 0.42 °C (7.90°C and 9.58 °C absolute temperatures). Most of the temperatures before ca. 2,000 cal a BP are cooler than present (9.16 °C) with only isolated centennial-scale periods where temperatures are warmer (Fig. 3). The centennial to interannual variability is, however, reduced in the last two millennia, which may be reflecting the switch to non-varved sediments at this time. The first millennium of the common era is slightly warmer than today remaining similar to present (Fig. 3).
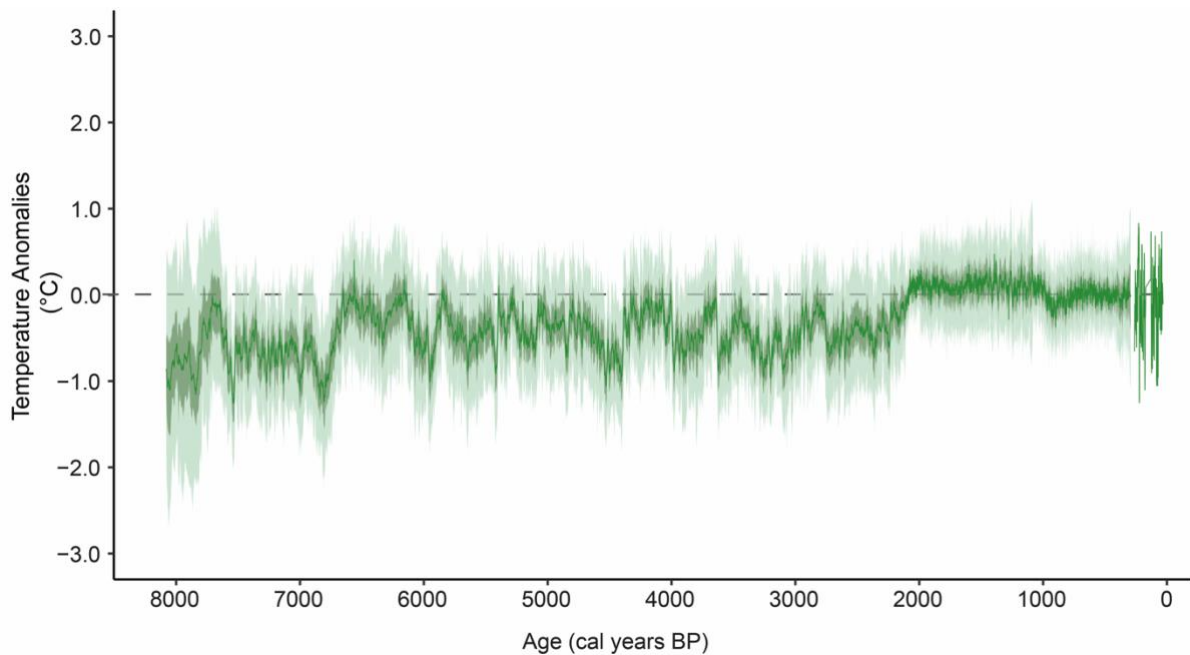

Figure 3: Annually resolved temperature reconstruction from Diss Mere. Dark green line represents the median reconstruction with 50th percentile and 95th percentile in darker green and light green, respectively. The data is presented in anomalies for the UK long-term average 1991-2020 and the dashed grey line marks the centred mean of 0 °C using this period.

4.2 Case site 2: Lake Nautajärvi, Southern Finland

We have applied the SCUBIDO approach to reconstruct Holocene annual mean temperature from Nautajärvi, a lake in southern Finland with a different lithology and sedimentation processes than Diss Mere. Lake Nautajärvi is also a varved lake but shows uninterrupted laminated sediments from the early Holocene to present (Ojala and Alenius, 2005). Except for the first 200 years of the record (9,852 – 9,625 cal a BP) when varves are thick (ca. 5 mm) due to a high detrital input during the formation of the lake (Ojala and Alenius, 2005; Ojala et al., 2008b), the sedimentation rate at Nautajärvi (0.2-1.6 mm/year) is similar to the varve thickness

of Diss Mere (0.1-1.4 mm/year). Analysis of both the sediments and the µXRF-CS data from Nautajärvi revealed that the lake, and subsequent sediment record is responsive to climate variability (Ojala et al., 2008a; Lincoln et al. 2025) thus is a good record to also apply this Bayesian methodology on. Table 1 summarises the characteristics of the modelling approach applied on lake Nautajärvi varved sediment sequence for full details about the µXRF-CS data from Nautajärvi please refer to Lincoln et al. (2025).

Table 1. Summary table of the Lake Nautajärvi data used for the Bayesian reconstruction. More information about the µXRF-CS instrument set up is presented in Lincoln et al. (2025).

	µXRF-CS set up	
µXRF-CS details	µXRF-CS elements used	Al, Si, S, K, Ca, Ti, V, Cr, Mn, Fe, Cu, Rb, Sr, and Zr
	Instrument set up	Sediments were scanned with a dwell time of 6 s, conducted using a Rh tube Rh-X-ray source operated at 30 kV and 60 mA.
Calibration data	Meteorological data	Temperature data for Nautajärvi was from 16 weather stations within a 200 km radius from the lake obtained gathered using the 'rnoaa' package (Chamberlain et al., 2024). Annual mean temperature is used. Data preservation from the interwar years (1918-1945) is limited and/or missing thus these have been excluded from the calibration dataset (Fig. S2)
	Age range	-70 to 68 cal a BP
	Number of time slices	102
Reconstruction data	Age range	69 to 9829 cal a BP
	Number of time slices	16418

511   Figure 4 shows the annual temperature reconstruction from Nautajärvi for the past ca.

512   9,800 years overlaid on top of the Diss Mere reconstruction. The average Holocene temperature

513   reconstructed from Nautajärvi is 5.1 °C (Fig. S4) and had a range of 1.60 °C between 4.22 °C

514   and 6.03 °C (-0.39 °C and 1.22 °C, anomalies) which is within the range of variability observed

515   during the instrumental period. Overall, the reconstructed Holocene temperatures at Nautajärvi

516   is cooler than present, except for the period between ca. 7,000 and 4,000 cal a BP where

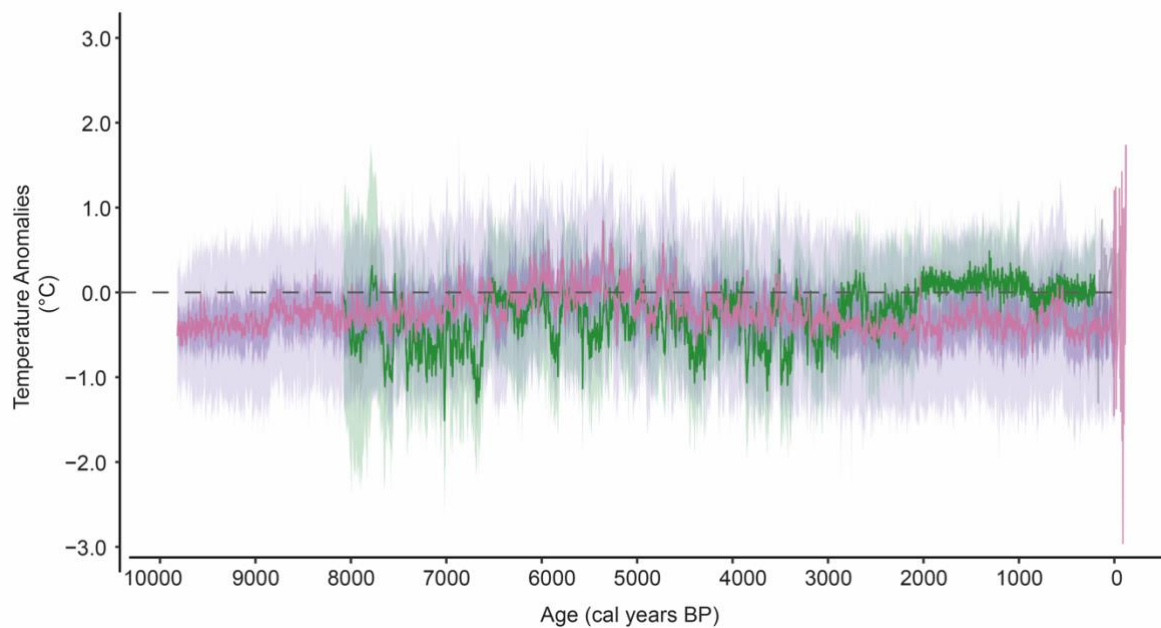517   temperatures are warmer and experience greater variability.

Figure 4. Annually resolved temperature reconstruction from Nautajärvi for the past ca 9,800 years (pink) overlaid on Diss Mere's reconstruction (green). Dark pink line represents the median reconstruction with 50th percentile and 95th percentile in darker pink and light pink, respectively. The anomalies are calculated with reference to the 1991-2020 mean from the instrumental data. The grey dashed line marks the 0 °C mean.

518

519   The comparison of Nautajärvi and Diss Mere through the Holocene shows slightly

520   different multi-millennial temperature evolutions where temperatures in England steadily

521   increase whereas Finland reaches maximum temperatures in the mid-Holocene and then

522   decreases thereafter (Fig. 4). We discuss millennial-scale trends in the next section when we

523   compare our reconstructions with published low-resolution Holocene temperature

524   reconstructions. On multi-decadal to centennial timescales, there is a good agreement between

525   the anomaly values at both sites showing similar trends and amplitude of change, especially

526   with the variability during the mid-Holocene from ca. 4,000 to 6,500 cal, yr BP (Fig. S5).

527   Larger variability in Diss Mere (England) prior to 6,500 cal yr BP compared to Nautajärvi

528   (Finland) might be reflecting different regional climate sensitivity during a period when the

529   instability of the Laurentide ice sheet and hydrological changes in the Baltic Sea region was

530   still having an important role on the reconfiguration of the climate system and spatial
531   distribution of climate patterns in the Northern Hemisphere (Yu and Harrison, 1995;
532   Wastegård, 2022).
533

4.3 Palaeoclimate comparisons

535   Neither Diss Mere nor Nautajärvi have previously published reconstructions of annual mean
536   temperature to compare to and test whether the temperatures produced from the SCUBIDO
537   modelling approach are sensible on longer timescales. Whilst there have been some
538   publications from these lake records which discuss climate variability, the proxies discussed
539   are either not interpreted as temperature (e.g. summer varve thickness from Diss Mere, Martin-
540   Puertas et al. 2023), reflect temperature in the summer season only (e.g. the Ca_{clr} record from
541   Diss Mere, Boyall et al. 2024), or reconstruct the Growing Degree Day (e.g. from Nautajärvi
542   in Ojala et al. 2008a) and thus may not capture the same variability and trends as our annual
543   mean temperature reconstructions. Therefore, we compare our reconstruction results with large
544   spatial multi-proxy reconstructions (Temp12k, Kaufman et al., 2020a) and data assimilation
545   results (LGMR, Osman et al., 2021; Holocene-DA, Erb et al., 2022) for the same period (Fig.
546   5). We choose these reconstructions to compare with because they are all based on large-scale
547   data compilations utilising a range of models and proxy types. The Temp12k and Holocene-
548   DA reconstructions both use the Temperature 12k proxy database (Kaufman et al., 2020b) with
549   the Temp-12k reconstruction using a multi-method ensemble to reconstruct temperatures at a
550   centennial resolution (Kaufman et al., 2020a) and the Holocene-DA using an updated version
551   of this dataset in a data assimilation framework to combine with transient climate simulations
552   in order to get a reconstruction of temperature at a decadal resolution (Erb et al., 2022). On the
553   other hand, the LGMR reconstruction uses only marine proxy records in a data assimilation
554   approach to produce a reconstruction of temperature at a multi-centennial resolution.
555   The multi-millennial trends in the reconstructions are best demonstrated with both Fig.
556   5a and b showing the clear evolution of temperatures through the Holocene. Fig. 5a shows the
557   slope from linear models conducted on the different reconstructions to explore the evolution of
558   temperature through time. The Diss Mere, Holocene-DA (Erb et al., 2022), and LGMR (Last
559   Glacial Maximum Reanalysis, Osman et al., 2021) linear models all demonstrate an
560   amelioration of temperature through the Holocene with similar rates of warming, especially
561   during the early to mid-Holocene where there are almost no differences between the records
562   (Fig. 5a). The Temp-12k reconstruction from Kaufman et al. (2020a) and the Nautajärvi

563 reconstruction from this study deviate from the general increasing trend observed in the other
564 reconstructions and instead show an overall decrease in temperature from the early to late
565 Holocene (Fig. 5a). These records have a more definitive early Holocene Thermal Maximum
566 (HTM) with cooling thereafter in comparison with the other reconstructions, hence the linear
567 model describing a general decrease in temperature through time. As part of the current
568 discussion on the Holocene temperature conundrum (Liu et al., 2020), the differences in
569 temperature evolution between the reconstructions may be a factor of a seasonal bias, which
570 has been already noted for the Temp-12k reconstruction reflecting mostly summer conditions
571 and/or spatial imbalances in proxy distributions, especially in the higher latitudes (Bova et al.,
572 2021; Erb et al., 2022).

573 The amplitude of variability from the SCUBIDO-produced reconstructions from this
574 study is much larger than the global reconstructions. Ultimately this is because the LGMR and
575 Temp12k have low temporal resolutions causing the reconstruction to be smoothed, and
576 contains a range of proxy types. Whilst the Holocene-DA reconstruction technically has data
577 every 10 years, as mentioned in their study, the reconstruction does not contain robust decadal
578 information from the proxy records and is achieved instead by utilising both proxy and transient
579 models together and thus the low amplitude is still inherent from the low-resolution proxy data
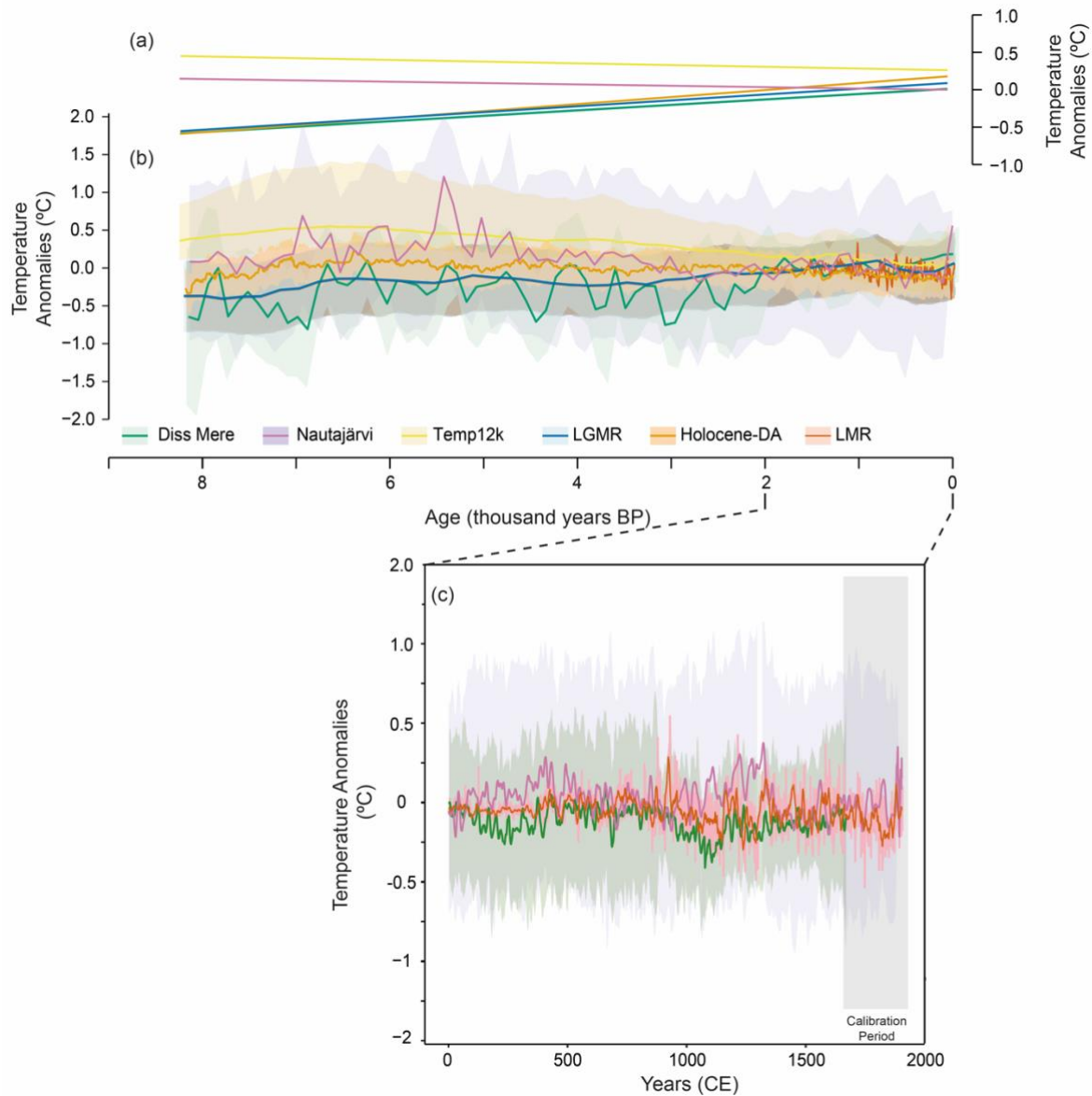580 used.

Figure 5: Comparison between different Holocene temperature reconstructions in anomalies. Note that the reference period for all these reconstructions is the mean between 2000 to 0 cal a BP. a) linear relationships between the reconstructed temperature and time for Diss Mere (green) Nautajärvi (purple), LGMR (Osman et al., 2021) (blue), Temp12k (Kaufman et al., 2020) (Yellow) and the Holocene-DA (Erb et al., 2022) (orange). b) The reconstructions from the above studies with Diss Mere and Nautajärvi resampled to 100 years to explore the centennial scale variability and match the resolution of the other reconstructions. The LGMR and Temp12k are presented at a 200-year. The envelopes for each line in the respective colours represent the uncertainty for each reconstruction. c) a focus window on the common era with the Diss Mere temperature reconstruction with the LMR (Tardif et al., 2019) (orange) for a grid 5°W:15°E, 50:60°N. The solid bold lines are at 10-year decadal moving average whereas the transparent envelopes are the original annual resolution.

581

4.3.1 The last two millennia

583 Reconstructing palaeoclimate for the Common Era (past 2,000 years) has been the focus of

584 many climate studies (e.g. Smerdon and Pollack, 2016; PAGES2k Consortium, 2017a; Tardif

585 et al., 2019; Anchukaitis and Smerdon, 2022). To test the Bayesian reconstructions from this

22

study through a period of increased anthropogenic disturbance, we compare the reconstructions to the Last Millennium Reanalysis (LMR, Tardif et al., 2019) (Fig. 5c). Whilst the LMR and the Bayesian reconstructions are annual, we decide to compare at a 10-year resolution to reduce noise and explore the main decadal-scale trends between each record. Despite increased anthropogenic disturbance to the lake system over the past 2,000 years at Diss Mere (Boyall et al., 2024), and a disruption to the proxy signal and lake functioning, the comparison between the overall trend of the LMR and Bayesian temperature reconstructions are good and show similar temporal evolutions (Fig. 5c).

In the first millennia (0-1000 CE), the LMR is much less variable than the Bayesian reconstructions, probably attributed to the very low number of proxy records used for the first few hundred years of the reconstruction (Tardif et al., 2019). Between ca. 500 and 1000 CE each of the reconstructions are very similar (Fig. 5c) and following 1000 CE temperatures decrease. There are some periodic increases in temperature at around 1100 – 1300 CE, mostly seen at Nautajärvi, but these might be reflecting the Medieval Climate Anomaly as they begin to decrease across all reconstructions at ca. 1300 CE.

The good consistency between the records highlights that despite the different sediment varve characteristics, varve formation processes, and interactions between sedimentation and human activity, the Bayesian approach is able to reconstruct a quantified, local to regional climate record from the µXRF-CS.

5.0 Conclusions and recommendations for future use of SCUBIDO

This study presents the first attempt at reconstructing quantitative annual mean temperatures from multivariate µXRF-data from sediment records using Bayesian inference. Several methodological decisions were made when building SCUBIDO which we believe can help contribute to the advancement of climate reconstructions within the community. The most important choice was to use Bayesian inference to not only get a single temperature estimate at each time point, but to also get a full posterior distribution to properly quantify uncertainties. In addition, we designed the model to include all geochemical elements and have SCUBIDO model their covariances instead of relying on prior assumptions about relationships, and the final choice was to synthesise SCUBIDO into an R package for the community. We believe that this was the best way to be as user friendly as possible as we think others could find this approach interesting and help make new annually resolved palaeoclimate reconstructions.

The ability of Bayesian in handling various types of data, changing timesteps/resolutions, and gaps within datasets has been utilised in this study, for example,

619   there are periods within both the µXRF-CS records from Diss Mere and Nautajärvi which have

620   short gaps and periods where the sedimentation rates are variable resulting in changing time

621   steps. However, this was easily mitigated against by using a Bayesian framework.

622   In this paper we apply SCUBIDO to two proxy records to reconstruct Holocene annual

623   mean temperature in Europe and the results showed consistency with previously published

624   paleoclimate reconstructions on a multi-millennial timescale. However, given the model and

625   the high-resolution proxy data from this study it provides a much more detailed overview of

626   temperature evolution through the Holocene by increasing the resolution to annual at a single

627   site. Of course, the records we compared to (Holocene-DA, Temp12k, and LGMR) have the

628   advantage of also being spatial reconstructions and not just temporal like in our study. The goal

629   would be for more people in the palaeoclimate community to use SCUBIDO and thus produce

630   more reconstructions of an annual resolution to then be incorporated into these large data

631   compilations.

632   Whilst we encourage other groups to use this approach on their µXRF-CS records, there

633   are some precautions which should be taken since SCUBIDO does not provide a physical

634   model between the climate and geochemical sediment composition. Like all palaeoclimate

635   reconstructions using different statistical techniques, there is still some assumption that the

636   proxy-climate relationship does not deviate too much through time to what is observed in the

637   calibration period. This is important to consider when sites have experienced substantial

638   alterations in human activity or other depositional changes, and we recommend to carefully

639   check that the major shifts in the climate reconstruction are explained from climate or rather

640   be explained by changes in the sedimentology (e.g. transitions from varved to non-varved

641   deposits and changes in the varve microfacies). Because of this, we encourage users to

642   qualitatively interpret their µXRF-CS records to see whether the lake remains sensitive to

643   climate through time, as well as finding the climate parameter to which the lake is sensitive to

644   and be cautious of the results if there are substantial human-induced changes to the µXRF-CS

645   record.

646   Finally, because µXRF-CS data is highly site-specific and sensitive to local systems, it

647   is not possible to calibrate one site and apply that calibration period on another µXRF-CS lake

648   record which may be common in other proxies e.g. pollen (Parnell et al., 2016).

649   Future developments of the SCUBIDO approach should include integrating age

650   uncertainty into the model as currently age ensembles are not used. This means that at present

651   lake data with stronger chronological age models would likely produce better reconstructions,

as aligning the calibration instrumental climate data with the correct layers of µXRF-CS data is important. This is an important consideration for future users who do not have a varve sequence or a tight chronology in their lake records. Another potential avenue for future development using SCUBIDO is to incorporate additional meteorological datasets and model them alongside temperature. Since other meteorological processes likely contribute to the noise in the reconstruction, capturing their joint dependencies may lead to improved reconstruction accuracy.

Author contribution

LB, AP, and AH, and CMP conceptualised the study. LB, AH, and AP created the methodology and software, LB made the R package. LB, AP, PL, AH, and CMP were involved in the discussion and formal analysis. CMP, PL, and AO were involved in data curation. LB wrote the original manuscript with supervision from AP and CMP and all authors were involved in the review and editing process.

Data Availability

The SCUBIDO R package was used to run the models and can be downloaded from the GitHub page: https://github.com/LauraBoyall/SCUBIDO. The µXRF-CS data for Diss Mere can be found here: https://zenodo.org/records/15168266, and Nautajarvi on Zenodo here: https://zenodo.org/records/14645779. The data used to compare the Diss Mere and Nautajärvi reconstructions to in Figure 5 are found at https://www.ncei.noaa.gov/access/paleo-search/study/29712 for the Temp12k reconstruction (Kaufman et al. 2020a), here (https://zenodo.org/records/6426332) for the Holocene-DA reconstruction from Erb et al. (2022), the LGMR reconstruction (Osman et al. 2021) can be found at https://www.ncei.noaa.gov/access/paleo-search/study/33112, and finally the LMR of Tardif et al. (2019) can be found at: https://atmos.washington.edu/~hakim/lmr/. The instrumental temperature dataset used to calibrate Diss Mere can be downloaded from: https://www.metoffice.gov.uk/hadobs/hadcet/data/download.html and the data to calibrate Nautajärvi was downloaded using the rnoaa R package (https://github.com/ropensci/rnoaa).

Competing interests

The authors declare that they have no conflict of interest.

Acknowledgements

Bibliography

Aitchison, J.: The statistical analysis of compositional data, Chapman & Hall, London, 1986.

Anchukaitis, K.J., and Smerdon, J.E.: Progress and uncertainties in global and hemispheric temperature reconstructions of the Common Era, Quat. Sci. Revs. 286, https://doi.org/10.1016/j.quascirev.2022.107537, 2022

Bader, J., Jungclaus, J., Krivova, N., Lorenz, S., Maycock, A., Raddatz, T., Schmidt, H., Toohey, M., Wu, C.-J., and Claussen, M.: Global temperature modes shed light on the Holocene temperature conundrum, Nat. Commun., 11, 4726, https://doi.org/10.1038/s41467-020-18478-6, 2020.

Birks, H. J. B.: Overview of numerical methods in palaeolimnology, in: Tracking Environmental Change Using Lake Sediments: Data Handling and Numerical Techniques, edited by: Birks, H. J. B., Lotter, A. F., Juggins, S., and Smol, J. P., Springer, Dordrecht, 19–92, 2012.

715 Boyall, L., Valcárcel, J. I., Harding, P., Hernández, A., and Martin-Puertas, C.: Disentangling
716 the environmental signals recorded in Holocene calcite varves based on modern lake
717 observations and annual sedimentary processes in Diss Mere, England, J. Paleolimnol., 70, 39–
718 56, https://doi.org/10.1007/s10933-023-00282-z, 2023.

720 Boyall, L., Martin-Puertas, C., Tjallingii, R., Milner, A.M., and Blockley, S.P.E.: Holocene
721 climate evolution and human activity as recorded by the sediment record of lake Diss Mere,
722 England. J. Quat. Sci. 39, 6, https://doi.org/10.1002/jqs.3646, 2024

724 Bova, S., Rosenthal, Y., Liu, Z., Godad, S. P., and Yan, M.: Seasonal origin of the thermal
725 maxima at the Holocene and the last interglacial, Nature, 589, 548–553,
726 https://doi.org/10.1038/s41586-020-03155-x, 2021.

728 Brooks, S. P. and Gelman, A.: General methods for monitoring convergence of iterative
729 simulations, J. Comput. Graph. Stat., 7, 434–455,
730 https://doi.org/10.1080/10618600.1998.10474787, 1998.

732 Burls, N. and Sagoo, N.: Increasingly sophisticated climate models need the out-of-sample
733 tests paleoclimates provide, J. Adv. Model. Earth Syst., 14, e2022MS003389,
734 https://doi.org/10.1029/2022MS003389, 2022.

736 Cahill, N., Croke, J., Campbell, M., Hughes, K., Vitkovsky, J., Kilgallen, J. E., and Parnell, A.:
737 A Bayesian time series model for reconstructing hydroclimate from multiple proxies,
738 Environmetrics, 34, e2786, https://doi.org/10.1002/env.2786, 2023.

740 Calvin, K., Dasgupta, D., Krinner, G., Mukherji, A., Thorne, P. W., Trisos, C., Romero, J.,
741 Aldunce, P., Barrett, K., Blanco, G., Cheung, W. W. L., Connors, S., Denton, F., Diongue-
742 Niang, A., Dodman, D., Garschagen, M., Geden, O., Hayward, B., Jones, C., Jotzo, F., Krug,
743 T., Lasco, R., Lee, Y.-Y., Masson-Delmotte, V., Meinshausen, M., Mintenbeck, K., Mokssit,
744 A., Otto, F. E. L., Pathak, M., Pirani, A., Poloczanska, E., Pörtner, H.-O., Revi, A., Roberts, D.
745 C., Roy, J., Ruane, A. C., Skea, J., Shukla, P. R., Slade, R., Slangen, A., Sokona, Y., Sörensson,
746 A. A., Tignor, M., Van Vuuren, D., Wei, Y.-M., Winkler, H., Zhai, P., Zommers, Z., Hourcade,
747 J.-C., Johnson, F. X., Pachauri, S., Simpson, N. P., Singh, C., Thomas, A., Totin, E., Arias, P.,
748 Bustamante, M., Elgizouli, I., Flato, G., Howden, M., Méndez-Vallejo, C., Pereira, J. J., Pichs-

749 Madruga, R., Rose, S. K., Saheb, Y., Sánchez Rodríguez, R., Ürge-Vorsatz, D., Xiao, C.,
750 Yassaa, N., Alegría, A., Armour, K., Bednar-Friedl, B., Blok, K., Cissé, G., Dentener, F.,
751 Eriksen, S., Fischer, E., Garner, G., Guivarch, C., Haasnoot, M., Hansen, G., Hauser, M.,
752 Hawkins, E., Hermans, T., Kopp, R., Leprince-Ringuet, N., Lewis, J., Ley, D., Ludden, C.,
753 Niamir, L., Nicholls, Z., Some, S., Szopa, S., Trewin, B., Van Der Wijst, K.-I., Winter, G.,
754 Witting, M., Birt, A., Ha, M., et al.: IPCC, 2023: Climate Change 2023: Synthesis Report.
755 Contribution of Working Groups I, II and III to the Sixth Assessment Report of the
756 Intergovernmental Panel on Climate Change [Core Writing Team, H. Lee and J. Romero
757 (eds.)], IPCC, Geneva, Switzerland, https://doi.org/10.59327/IPCC/AR6-9789291691647,
758 2023.

759

760 Cartapanis, O., Jonkers, L., Moffa-Sanchez, P., Jaccard, S.L., and de Vernal, A.: Complex
761 spatio-temporal structure of the Holocene Thermal Maximum. Nature. Comms. 13, 5662,
762 https://doi.org/10.1038/s41467-022-33362-1, 2022.

763

764 Cassou, C., Kushnir, Y., Hawkins, E., Pirani, A., Kucharski, F., Kand, I-S., and Caltabiano, N.:
765 Decadal climate variability and predictability: Challenges and opportunities. Bul. Ameri. Met.
766 Soc. 99(3), 479-490. https://doi.org/10.1175/BAMS-D-16-0286.1, 2018.

767

768 Chamberlain, S., Hocking, D., Anderson, B., Salmon, M., Erickson, A., Potter, N., Stachelek,
769 J., Simmons, A., Ram, K., and Edmund, H. rnoaa: 'NOAA weather data from R. R package
770 version 1.4.0. https://github.com/ropensci/rnoaa

771

772 Chevalier, M., Davis, B. A. S., Heiri, O., Seppä, H., Chase, B. M., Gajewski, K., Lacourse, T.,
773 Telford, R., Finsinger, W., Guiot, J., Kühl, N., Maezumi, S. Y., Tipton, J., Carter, V., Brussel,
774 T., Phelps, L., Dawson, A., Zanon, M., Vallé, F., Nolan, C., Mauri, A., de Vernal, A., Izumi,
775 K., Holmström, L., Marsicek, J., Goring, S., Sommer, P., Chaput, M., and Kupriyanov, D.:
776 Pollen-based climate reconstruction techniques for late Quaternary studies, Earth Sci. Rev.,
777 210, 1–33, https://doi.org/10.1016/j.earscirev.2020.103384, 2020.

778

779 Chu, P-S., Zhao, X.: Bayesian analysis for extreme climatic events: A review, Atmos. Res.
780 102. https://doi.org/10.1016/j.atmosres.2011.07.001, 2011.

781

782   Davis, B. A. S., Brewer, S., Stevenson, A. C., and Guiot, J.: The temperature of Europe during
783   the Holocene reconstructed from pollen data, Quat. Sci. Rev., 22, 1701–1716,
784   https://doi.org/10.1016/S0277-3791(03)00173-2, 2003.
785

786   Davies, S. J., Lamb, H. F., and Roberts, S. J.: Micro-XRF core scanning in palaeolimnology:
787   recent developments, in: Micro-XRF Studies of Sediment Cores: Applications of a Non-
788   Destructive Tool for the Environmental Sciences, edited by: Croudace, I. W. and Rothwell, R.
789   G., Developments in Paleoenvironmental Research, Springer, Dordrecht, 189–226,
790   https://doi.org/10.1007/978-94-017-9849-5_7, 2015.
791

792   Erb, M. P., McKay, N. P., Steiger, N., Dee, S., Hancock, C., Ivanovic, R. F., Gregoire, L. J.,
793   and Valdes, P.: Reconstructing Holocene temperatures in time and space using paleoclimate
794   data assimilation, Clim. Past., 18, 2599–2629, https://doi.org/10.5194/cp-18-2599-2022, 2022.
795

796   Esper, J., Smerdon, J.E., Anchukaitis, K.J., Allen, K., Cook, E.R., D'Arrigo, R., Guillet, S.,
797   Ljunggvist, F.C., Reinig, F., Schneider, L., Sigl, M., Stoffel, M., Trnka, M., Wilson and
798   Büntgen, U.: The IPCC's reductive Common Era temperature history. Commun Earth Environ
799   5, 222, https://doi.org/10.1038/s43247-024-01371-1, 2024.
800

801   Gelman, A. and Rubin, D. B.: Inference from iterative simulation using multiple sequences,
802   Stat. Sci., 7, 457–472, https://doi.org/10.1214/ss/1177011136, 1992.
803

804   Gelman, A., Carlin, J. B., Stern, H. S., and Rubin, D. B.: Bayesian data analysis, 2008.
805

806   Haslett, J., Whiley, M., Bhattacharya, S., Salter-Townshend, M., Wilson, S. P., Allen, J. R. M.,
807   Huntley, B., and Mitchell, F. J. G.: Bayesian palaeoclimate reconstruction, J. R. Stat. Soc. Ser.
808   A Stat. Soc., 169, 395–438, 2006.
809

810   Hernández, A., Sánchez-López, G., Pla-Rabes, S., Comas-Bru, L., Parnell, A., Cahill, N.,
811   Geyer, A., Trigo, R. M., and Giralt, S.: A 2,000-year Bayesian NAO reconstruction from the
812   Iberian Peninsula, Sci. Rep., 10, 14961, https://doi.org/10.1038/s41598-020-71372-5, 2020.
813

Holmström, L., Ilvonen, L., Seppä, H., and Veski, S.: A Bayesian spatiotemporal model for reconstructing climate from multiple pollen records, Ann. Appl. Stat., 9, 1194–1225, https://doi.org/10.1214/15-AOAS832, 2015.

Imbrie, J. and Kipp, N. G.: A new micropaleontological method for quantitative paleoclimatology: application to a late Pleistocene Caribbean core, in: The Late Cenozoic Glacial Ages, edited by: Turekian, K. K., Yale University Press, New Haven, 71–181, 1971.

Jiang, W., Guiot, J., Chu, G., Wu, H., Yuan, B., Hatté, C., and Guo, Z.: An improved methodology of the modern analogues technique for palaeoclimate reconstruction in arid and semi-arid regions, Boreas, 39, 145–153, https://doi.org/10.1111/j.1502-3885.2009.00115.x, 2010.

Jones, P. D., Briffa, K. R., Osborn, T. J., Lough, J. M., van Ommen, T. D., Vinther, B. M., Luterbacher, J., Wahl, E. R., Zwiers, F. W., Mann, M. E., Schmidt, G. A., Ammann, C. M., Buckley, B. M., Cobb, K. M., Esper, J., Goosse, H., Graham, N., Jansen, E., Kiefer, T., Kull, C., Küttel, M., Mosley-Thompson, E., Overpeck, J. T., Riedwyl, N., Schulz, M., Tudhope, A. W., Villalba, R., Wanner, H., Wolff, E., and Xoplaki, E.: High-resolution palaeoclimatology of the last millennium: a review of current status and future prospects, The Holocene, 19, 3–49, https://doi.org/10.1177/0959683608098952, 2009.

Juggins, S. and Birks, H. J. B.: Quantitative environmental reconstructions from biological data, in: Tracking Environmental Change Using Lake Sediments: Data Handling and Numerical Techniques, edited by: Birks, H. J. B., Lotter, A. F., Juggins, S., and Smol, J. P., Springer Netherlands, Dordrecht, 431–494, https://doi.org/10.1007/978-94-007-2745-8_14, 2012.

Kageyama, M., Braconnot, P., Harrison, S. P., Haywood, A. M., Jungclaus, J. H., Otto-Bliesner, B. L., Peterschmitt, J.-Y., Abe-Ouchi, A., Albani, S., Bartlein, P. J., Brierley, C., Crucifix, M., Dolan, A., Fernandez-Donado, L., Fischer, H., Hopcroft, P. O., Ivanovic, R. F., Lambert, F., Lunt, D. J., Mahowald, N. M., Peltier, W. R., Phipps, S. J., Roche, D. M., Schmidt, G. A., Tarasov, L., Valdes, P. J., Zhang, Q., and Zhou, T.: The PMIP4 contribution to CMIP6 – Part 1: Overview and over-arching analysis plan, Geosci. Model Dev., 11, 1033–1057, https://doi.org/10.5194/gmd-11-1033-2018, 2018.

848

849 Kaufman, D., Mckay, N., Routson, N., Erb, M., Dätwyler, C., Sommer, P.S., and Davis, D.:

850 Holocene global mean surface temperature, a multi-method reconstruction approach. Sci. Data,

851 7, 201, https://doi.org/10.1038/s41597-020-0530-7. 2020a

852

853 Kaufman, D., McKay, N., Routson, C., Erb, M., Davis, B., Heiri, O., Jaccard, S., Tierney, J.,

854 Dätwyler, C., Axford, Y., Brussel, T., Cartapanis, O., Chase, B., Dawson, A., de Vernal, A.,

855 Engels, S., Jonkers, L., Marsicek, J., Moffa-Sánchez, P., Morrill, C., Orsi, A., Rehfeld, K.,

856 Saunders, K., Sommer, P. S., Thomas, E., Tonello, M., Tóth, M., Vachula, R., Andreev, A.,

857 Bertrand, S., Biskaborn, B., Bringué, M., Brooks, S., Caniupán, M., Chevalier, M., Cwynar,

858 L., Emile-Geay, J., Fegyveresi, J., Feurdean, A., Finsinger, W., Fortin, M.-C., Foster, L., Fox,

859 M., Gajewski, K., Grosjean, M., Hausmann, S., Heinrichs, M., Holmes, N., Ilyashuk, B.,

860 Ilyashuk, E., Juggins, S., Khider, D., Koinig, K., Langdon, P., Larocque-Tobler, I., Li, J.,

861 Lotter, A., Luoto, T., Mackay, A., Magyari, E., Malevich, S., Mark, B., Massaferro, J.,

862 Montade, V., Nazarova, L., Novenko, E., Pařil, P., Pearson, E., Peros, M., Pienitz, R.,

863 Płóciennik, M., Porinchu, D., Potito, A., Rees, A., Reinemann, S., Roberts, S., Rolland, N.,

864 Salonen, S., Self, A., Seppä, H., Shala, S., St-Jacques, J.-M., Stenni, B., Syrykh, L., Tarrats, P.,

865 Taylor, K., van den Bos, V., Velle, G., Wahl, E., Walker, I., Wilmshurst, J., Zhang, E., and

866 Zhilich, S.: A global database of Holocene paleotemperature records, Sci. Data, 7, 115,

867 https://doi.org/10.1038/s41597-020-0445-3, 2020b.

868

869 Kaufman, D. S. and McKay, N. P.: Technical Note: Past and future warming – direct

870 comparison on multi-century timescales, Clim. Past., 18, 911–917, https://doi.org/10.5194/cp-

871 18-911-2022, 2022.

872

873 Lincoln, P., Tjallingii, R., Kosonen, E., Ojala, A., Abrook, A.M., and Martin-Puertas, C.:

874 Disruption of boreal lake circulation in response to mid-Holocene warmth; Evidence from the

875 varved sediments of Lake Nautajärvi, southern Finland. Sci. Tot. Enviro. In revision.

876

877 Liu, M., Prentice, I. C., ter Braak, C. J. F., and Harrison, S. P.: An improved statistical approach

878 for reconstructing past climates from biotic assemblages, Proc. Math. Phys. Eng. Sci., 476,

879 20200346, https://doi.org/10.1098/rspa.2020.0346, 2020.

880

881 Liu, Z., Zhu, J., Rosenthal, Y., Zhang, X., Otto-Bliesner, B. L., Timmermann, A., Smith, R. S.,

882 Lohmann, G., Zheng, W., and Elison Timm, O.: The Holocene temperature conundrum, Proc.

883 Natl. Acad. Sci., 111, E3501–E3505, https://doi.org/10.1073/pnas.1407229111, 2014.

884

885 Martin-Puertas, C., Walsh, A. A., Blockley, S. P. E., Harding, P., Biddulph, G. E., Palmer, A.,

886 Ramisch, A., and Brauer, A.: The first Holocene varve chronology for the UK: based on the

887 integration of varve counting, radiocarbon dating and tephrostratigraphy from Diss Mere (UK),

888 Quat. Geochronol., 61, 101134, https://doi.org/10.1016/j.quageo.2020.101134, 2021.

889

890 Martin-Puertas, C., Hernandez, A., Pardo-Igúzquiza, E., Boyall, L., Brierley, C., Jiang, Z.,

891 Tjallingii, R., Blockley, S.P.E., and Rodríguez-Tovar, F.J.: Dampened predictable decadal

892 North Atlantic climate fluctuations due to ice melting, Nat. Geosci., 16, 357–362,

893 https://doi.org/10.1038/s41561-023-01145-y, 2023.

894

895 Mauri, A., Davis, B.A.S., Collins, P.M., and Kaplan, J.O. The climate of Europe during the

896 Holocene: a gridded pollen-based reconstruction and its multi-proxy evaluation. Quat. Sci.

897 Revs, 112, 109-127, https://doi.org/10.1016/j.quascirev.2015.01.013, 2015.

898

899 Met Office Hadley Centre: HadCET: Central England Temperature Data, available at:

900 https://www.metoffice.gov.uk/hadobs/hadcet/data/download.html, last access: 4th November

901 2024.

902

903 Ojala, A. E. K. and Alenius, T.: 10,000 years of interannual sedimentation recorded in the Lake

904 Nautajärvi (Finland) clastic–organic varves, Palaeogeogr. Palaeoclimatol. Palaeoecol., 219,

905 285–302, https://doi.org/10.1016/j.palaeo.2005.01.002, 2005.

906

907 Ojala, A.E.K., Alenius, T., Seppä, H., and Giesecke, T.: Integrated varve and pollen-based

908 temperature reconstruction from Finland: evidence for Holocene seasonal temperature patterns

909 at high latitudes. The Holocene. https://doi.org/10.1177/0959683608089207, 2008a.

910

911 Ojala, A.E.K. Heinsalu, A., Kauppila, T., Alenius, T., and Saarnisto, M. Characterising

912 changes in the sedimentary environment of a varved lake sediment record in southern central

913 Finland around 8000 cal. yr BP. J. Quat. Sci. 23(8), 765-775. https://doi.org/10.1002/jqs.1157,

914 2008b

Osman, M. B., Tierney, J. E., Zhu, J., Tardif, R., Hakim, G. J., King, J., and Poulsen, C. J.: Globally resolved surface temperatures since the Last Glacial Maximum, Nature, 599, 239–244, https://doi.org/10.31223/X5S31Z, 2021.

PAGES2k Consortium: A global multiproxy database for temperature reconstruction of the Common Era, Scient. Data, 4, 170088, https://doi.org/10.1038/sdata.2017.88, 2017a.

PAGES 2k Consortium: Consistent multidecadal variability in global temperature reconstructions and simulations over the Common Era. Nat. Geosci. https://doi.org/10.1038/s41561-019-0400-0, 12, 643–649, 2019.

Parnell, A. C., Sweeney, J., Doan, T. K., Salter-Townshend, M., Allen, J. R. M., Huntley, B., and Haslett, J.: Bayesian inference for palaeoclimate with time uncertainty and stochastic volatility, J. R. Stat. Soc. Ser. C Appl. Stat., 64, 115–138, 2015.

Parnell, A.C., Haslett, J., Sweeney, J., Doan, T.K., Allen, J.R.M., and Huntley, B.: Joint palaeoclimate reconstruction from pollen data via forward models and climate histories. Quat. Sci. Revs, 151, 1, https://doi.org/10.1016/j.quascirev.2016.09.007, 2016.

Peti, L. and Augustinus, P. C.: Micro-XRF-inferred depositional history of the Orakei maar lake sediment sequence, Auckland, New Zealand, J. Paleolimnol., 67, 327–344, https://doi.org/10.1007/s10933-022-00235-y, 2022.

Plummer, M.: JAGS: A program for analysis of Bayesian graphical models using Gibbs sampling, in: Proceedings of the 3rd International Workshop on Distributed Statistical Computing (DSC 2003), Vienna, Austria, 20–22 March 2003, available at: https://www.r-project.org/conferences/DSC-2003/Proceedings/Plummer.pdf, last access: 1st November 2024.

Rasmussen, S. O., Vinther, B. M., Clausen, H. B., and Andersen, K. K.: Early Holocene climate oscillations recorded in three Greenland ice cores, Quat. Sci. Rev., 26, 1907–1914, https://doi.org/10.1016/j.quascirev.2007.06.015, 2007.

948 Smerdon, J. E. and Pollack, H. N.: Reconstructing Earth's surface temperature over the past
949 2000 years: the science behind the headlines, Wiley Interdiscip. Rev. Clim. Change,
950 https://doi.org/10.1002/wcc.418, 2016.

952 Snyder, C. W.: The value of paleoclimate research in our changing climate, Clim. Change, 100,
953 407–418, https://doi.org/10.1007/s10584-010-9842-5, 2010.

955 Su, Y.-S. and Yajima, M.: R2jags: Using R to run 'JAGS', R package version 0.7-1, available
956 at: https://cran.r-project.org/web/packages/R2jags/index.html, last access: 4th November 2024

958 Sweeney, J., Salter-Townshend, M., Edwards, T., Buck, C. E., and Parnell, A. C.: Statistical
959 challenges in estimating past climate changes, WIREs Comput. Stat., 10, e1437,
960 https://doi.org/10.1002/wics.1437, 2018.

962 Tardif, R., Hakim, G. J., Perkins, W. A., Horlick, K. A., Erb, M. P., Emile-Geay, J., Anderson,
963 D. M., Steig, E. J., and Noone, D.: Last Millennium Reanalysis with an expanded proxy
964 database and seasonal proxy modeling, Clim. Past, 15, 1251–1273, https://doi.org/10.5194/cp-
965 15-1251-2019, 2019.

967 ter Braak, C. J. F., Juggins, S., Birks, H. J. B., and van der Voet, H.: Weighted averaging partial
968 least squares regression (WA-PLS): definition and comparison with other methods for species-
969 environment calibration, in: Multivariate Environmental Statistics, edited by: Patil, G. P., and
970 Rao, C. R., Elsevier Science Publishers B.V. (North-Holland), Amsterdam, 525–560, 1993.

972 Tierney, J. E., Malevich, S. B., Gray, W., Vetter, L., and Thirumalai, K.: Bayesian calibration
973 of the Mg/Ca paleothermometer in planktic foraminifera, Paleoceanogr. Paleoclimatol., 34,
974 2005–2030, https://doi.org/10.1029/2019PA003744, 2019.

976 Tingley, M. P., Craigmile, P. F., Haran, M., Li, B., Mannshardt, E., and Rajaratnam, B.: Piecing
977 together the past: statistical insights into paleoclimatic reconstructions, Quat. Sci. Rev., 35, 1–
978 22, https://doi.org/10.1016/j.quascirev.2012.01.012, 2012.

Tingley, M. P. and Huybers, P.: A Bayesian algorithm for reconstructing climate anomalies in space and time. Part I: Development and applications to paleoclimate reconstruction problems, J. Clim., 23, 2759–2781, https://doi.org/10.1175/2009JCLI3015.1, 2010.

Tjallingii, R., Röhl, U., Kölling, M., and Bickert, T.: Influence of the water content on X-ray fluorescence core-scanning measurements in soft marine sediments, Geochem. Geophys. Geosyst., 8, Q02004, https://doi.org/10.1029/2006GC001393, 2007.

van de Schoot, R., Depaoli, S., King, R., Kramer, B., Märtens, K., Tadesse, M. G., Vannucci, M., Gelman, A., Veen, D., Willemsen, J., and Yau, C.: Bayesian statistics and modelling, Nat. Rev. Methods Primers, 1, 1–26, https://doi.org/10.1038/s43586-020-00001-2, 2021.

Vehtari, A., Gelman, A., Simpson, D., Carpenter, B., and Bürkner, P. C.: Rank-normalization, folding, and localization: an improved for assessing convergence of MCMC (with discussion), Bayesian Anal., 16, 667–718, https://doi.org/10.1214/20-BA1221, 2021.

Wastegård, S. The Holocene of Sweden – a review. GFF. https://doi.org/10.1080/11035897.2022.2086290.

Wegmann, M., and Jaume-Santero, F.: Artificial intelligence achieves easy-to-adapt nonlinear global temperature reconstructions using minimal local data. Comms. Earth. Enviro, 4, 217, https://doi.org/10.1038/s43247-023-00872-9, 2023.

Weltje, G. J. and Tjallingii, R.: Calibration of XRF core scanners for quantitative geochemical logging of sediment cores: theory and application, Earth Planet. Sci. Lett., 274, 423–438, https://doi.org/10.1016/j.epsl.2008.07.054, 2008.

Weltje, G. J., Bloemsma, M. R., Tjallingii, R., Heslop, D., Röhl, U., and Croudace, I. W.: Prediction of geochemical composition from XRF core scanner data: a new multivariate approach including automatic selection of calibration samples and quantification of uncertainties, in: Micro-XRF Studies of Sediment Cores: Applications of a Non-Destructive Tool for the Environmental Sciences, edited by: Croudace, I. W. and Rothwell, R. G., Springer Netherlands, Dordrecht, 507–534, https://doi.org/10.1007/978-94-017-9849-5_21, 2015.

1014 Yu, G., and Harrison, S.: Holocene changes in atmospheric circulation patterns as shown by

1015 lake status changes in northern Europe. Boreas. 24, 3, 260-258, https://doi.org/10.1111/j.1502-

1016 3885.1995.tb00778.x, 1995.

1017

1018 Zander, P.D., Żarczyński, M., Tylmann, W., Vogel, H., and Grosjean, M.: Subdecadal

1019 Holocene warm-season temperature variability in Central Europe recorded by biochemical

1020 varves. Geophys. Res. Lett. 51. https://doi.org/10.1029/2024GL110871 , 2024.

1021

1022 Zolitschka, B., Francus, P., Ojala, A.E.K., and Schimmelmann, A.: Varves in lake sediments –

1023 a review. Quat. Sci. Revs, 117, 1-41, http://dx.doi.org/10.1016/j.quascirev.2015.03.019, 2015.